

# Sensitivity Analysis of Singlet Vector-Like $B$ Quarks via Photon-Induced Processes at FCC $\mu p$

Eda Alici

Received: date / Accepted: date

**Abstract** This study presents a dedicated and systematic sensitivity analysis of a singlet-type vector-like  $B$  quark at an FCC- $\mu p$  collider with a center-of-mass energy of  $\sqrt{s} = 24.5$  TeV via photon-induced production mechanisms. The analyses are based on the  $B \rightarrow Zb$  decay and the lepton decay of the  $Z$  boson on a clean and selective final state. In this regard, we observed that the applied kinematic cuts suppress the Standard Model backgrounds by several orders of magnitude while maintain high signal efficiency. Also, the obtained results show that for  $\mathcal{L} = 1000 \text{ fb}^{-1}$ , even small coupling constant values in the mass range  $M_B = 2\text{--}3$  TeV are accessible. In this context, an exclusion limit of  $g^* \simeq 0.12\text{--}0.17$  at 95% confidence level and a sensitivity in the range of  $g^* \simeq 0.22\text{--}0.30$  for the  $5\sigma$  discovery region are obtained. Moreover, the calculations indicate that scenarios with smaller  $\text{BR}(B \rightarrow Zb)$  values via increasing integrated luminosity values can be experimentally tested. As a result, the outputs of the study show that the FCC- $\mu p$  environment offers a unique and powerful discovery potential for vector-like quark searches that go beyond the current LHC limits and complement the decreasing sensitivity of the ep and  $e^+e^-$  colliders in the high-mass regime. In this context, the findings suggest that the  $\mu p$  colliders can be considered not only as a complementary option for the search of heavy new particles in the future accelerator programme, but also as a strategic discovery tool.

**Keywords** VLQ · Photon-induced production · FCC- $\mu p$  · BSM physics · Future colliders

Department of Physics, Zonguldak Bülent Ecevit University, Zonguldak, Turkey

## 1 Introduction

The Standard Model (SM) successfully explains a large portion of the high-precision particle physics experiments conducted to date. However, the SM fails to provide satisfactory solutions to some fundamental problems. Problems such as the mass hierarchy problem, the absence of dark matter candidates, baryon asymmetry, and the origin of neutrino masses are some of the extremely important shortcomings of the SM. These shortcomings necessitate the search for new physics scenarios beyond the SM. In this context, many new physics scenarios are being intensively investigated both theoretically and experimentally. At this point, Vector-Like Quarks (VLQs) are among the candidates for new fermions with strong theoretical motivation and appear naturally in many extended models. [1, 2].

As it is well known, the left- and right-handed components of VLQs have the same transformation properties under electroweak representations. Therefore, VLQ masses can be directly generated via Dirac mass terms and these masses are not necessarily dependent on the Higgs mechanism. This characteristic contributes to alleviate the hierarchy problem and also facilitates the control of the flavor structure. For these reasons, VLQs stand out as attractive particles in theoretical research. On the other hand, VLQs are classified into types  $T$ ,  $B$ ,  $X$  and  $Y$  according to their electromagnetic charges and electroweak quantum numbers. Furthermore, these different types of VLQs can appear as singlet or doublet under  $SU(2)_L$  gauge symmetry.

There are many phenomenological studies on VLQs in the literature. These studies cover different electroweak representations, production mechanisms and decay channels. Existing analyses deal with both single and pair production processes at hadron, lepton and lepton-hadron

colliders [3–35]. In the present work, we investigate the VLQ- $(B)$  with electric charge  $Q_B = -1/3$  and singlet representation  $SU(2)_L$ . Here, VLQ- $(B)$  interacts with SM quarks via mixing. This mixing allows three main decay channels for the  $B$  quark:

$$B \rightarrow Wt, \quad B \rightarrow Zb, \quad B \rightarrow Hb \quad (1)$$

In the heavy mass limit, the branching ratios of these channels are approximately  $\text{BR}(B \rightarrow Wt) : \text{BR}(B \rightarrow Zb) : \text{BR}(B \rightarrow Hb) \simeq 2 : 1 : 1$  order. This universal behavior can be explained by Goldstone's equivalence theorem. However, the exact ratios depend on the mixing structure and model-specific interactions, and these ratios may vary accordingly [2, 25, 36, 37].

In the simplified model used in this paper, the effective coupling parameter  $g^*$  determines the overall coupling scale of all interactions of the VLQ- $B$  quark with SM fermions and electroweak bosons. On the other hand, the parameter  $R_L$  describes the relative mixing structure of the VLQ- $B$  quark between light up-type quarks ( $u, c$ ) and third generation quarks. Here, the choice of  $R_L = 0.05$  ensures that the branching ratios of the  $B$  quark are approximately in the order of 2:1:1 given above. In this scenario, the single generation process predominantly occurs via light up-type quarks, while the decay dynamics are mainly determined by third-generation quarks [30, 38]. This study focuses on the  $B \rightarrow Zb$  decay channel. This choice is motivated by the fact that this channel provides an experimentally clean reconstruction and offers clear advantages in terms of signal-to-background separation. These advantages become even more pronounced when the leptonic decay channel of the  $Z$  boson is preferred. This is because the leptonic  $Z$  decay ( $Z \rightarrow \ell^+ \ell^-$ ) allows for clear observation of heavy resonances due to its low SM background and high invariant mass resolution [7]. The combination of these properties makes the  $Zb$  channel a highly selective and powerful signal in the  $\mu p$  collider environment. These properties have led the  $B \rightarrow Zb$  channel to assume a central role in the search for the VLQ- $B$  quark. In this context, many studies have been reported in the literature, covering both pair production and singlet production of VLQ- $B$  quarks at different types of colliders in detail. Among these, in studies on hadron colliders, single production processes in  $pp$  collisions via the  $B \rightarrow Zb$  channel have been extensively investigated. At this point, for the 14 TeV LHC and future higher-energy hadron machines, discovery and exclusion potentials in the  $g^*$  and  $M_B$  parameter spaces have been reported [9, 25, 39]. This relevant literature shows that single production becomes more dominant than pair production, especially in the high-mass regime. It also reveals that the sensitivity to coupling

parameters plays a decisive role [4, 26–28]. On the other hand, phenomenological studies on Lepton-hadron colliders have investigated the single production of singlet  $B$  quarks in  $ep$  machines such as LHeC and FCC-eh. These studies have reported that sensitivities up to  $M_B \sim 1.4\text{--}2.2$  TeV can be achieved in the  $B \rightarrow Zb$  and  $B \rightarrow Hb$  channels [30–32]. Also, in phenomenological studies on linear lepton–lepton colliders of the  $e^+e^-$  type, especially in the 3 TeV CLIC scenario, single  $B$  production has been investigated up to around  $M_B \sim 2$  TeV [33–35].

On the other hand, on the experimental side, analyses have been performed by the ATLAS and CMS collaborations using LHC Run-2 ( $\sqrt{s} = 13$  TeV) data. These analyses excluded approximately the  $M_B \lesssim 1.2\text{--}1.6$  TeV range for the singlet  $B$  quark at a 95% confidence level via the pair production channel [40–44]. Furthermore, in single production analyses, it was shown that the obtained exclusion limits were strongly dependent on the coupling parameters. It was moreover determined that these limits were generally confined to lower mass regions [40, 44]. These findings reveal that achieving a heavy-mass regime in current hadron colliders remains limited. This indicates that it is important to investigate alternative collider environments. In this context, muon-proton ( $\mu p$ ) colliders, especially when considered in conjunction with FCC infrastructure, stand out as a strong alternative for the search for new heavy particles thanks to their high centre of mass energies and clean initial states [45–48]. In this context, it can be predicted that the high centre of mass energies, such as  $\sqrt{s} = 24.5$  TeV, projected for FCC-based  $\mu p$  machines, will enable photon-induced processes to function even in the heavy-mass regime [49]. At this point, although there are various studies in the literature on contact interactions, anomalous coupling structures, and excited leptons in the FCC- $\mu p$  environment, a detailed analysis focusing on the photon-induced single generation of the singlet VLQ- $B$  quark, and in particular on the  $B \rightarrow Zb$  channel has not yet been reported.

Based on the significant literature mentioned above, this study investigates the single production of singlet-type VLQ- $B$  via photon-proton interactions at the FCC- $\mu p$  collider with centre-mass energy of  $\sqrt{s} = 24.5$  TeV. To this end, the paper is organized as follows: Section 2 introduces the theoretical framework and presents the effective Lagrangian describing the interactions of the singlet vector-like  $B$  quark. In Section 2.1, the signal process and the corresponding final state topology are described. Section 2.2 details the event generation procedure, simulation setup, Standard Model background processes, and the event selection strategy. The statis-

tical methodology and sensitivity analysis for discovery and exclusion are discussed in Section 2.4. Finally, Section 3 summarizes the main results and provides concluding remarks and future perspectives.

## 2 Model Definition and Effective Lagrangian

In this study, the interactions of the singlet-type vector-like  $B$  quark with SM fermions and electroweak bosons are defined by the following effective Lagrangian within the framework of the effective theory approach [1, 2, 38, 50]:

$$\mathcal{L}_{\text{int}} = \frac{g g^*}{\sqrt{2}} \left[ \sqrt{\frac{R_L}{1+R_L}} \bar{B}_L \gamma^\mu W_\mu^- u_L + \sqrt{\frac{R_L}{1+R_L}} \bar{B}_L \gamma^\mu W_\mu^- c_L \right. \\ + \sqrt{\frac{1}{1+R_L}} \bar{B}_L \gamma^\mu W_\mu^- t_L \\ + \sqrt{\frac{1}{1+R_L}} \frac{1}{2 \cos \theta_W} \bar{B}_L \gamma^\mu Z_\mu b_L \\ \left. - \sqrt{\frac{1}{1+R_L}} \frac{m_B}{2m_W} \bar{B}_R H b_L \right] + \text{h.c.} \quad (2)$$

where  $g$  is the  $SU(2)_L$  weak coupling constant,  $g^*$  is the effective coupling parameter pertaining to new physics,  $\theta_W$  is the Weinberg angle,  $m_B$  is the mass of the vector-like  $B$  quark, and  $m_W$  is the mass of the  $W$  boson.  $u_L$ ,  $c_L$ ,  $t_L$  and  $b_L$  represent the left-handed components of the SM up, down, top and bottom quarks, respectively;  $W_\mu^-$  and  $Z_\mu$  represent the electroweak gauge bosons; and  $H$  represents the physical Higgs boson field. Here, "h.c." denotes the Hermitian conjugate terms.

Also, in the equation,  $(R_L)$ , the mixing parameter, between light up-type quarks ( $u, c$ ) and third-generation quarks is described via decay widths as follows,

$$R_L = \frac{\Gamma(B \rightarrow u, c)}{\Gamma(B \rightarrow t)} \quad (3)$$

as defined in [2, 25, 38]. In this work, the mixing parameter is fixed as  $R_L = 0.05$

This choice ensures that the production of the  $B$  quark occurs predominantly via light up-type quarks, while the decay dynamics are determined primarily by the third-generation down quark ( $b$ ). Thus, the production and decay processes can be parametrically distinguished, and the photon-induced single production mechanism can be analysed in a simpler way.

It is known that the additional interactions and new fermion partners that arise in the doublet or higher representations make the analysis topology and background structure more complex. On the other hand, the singlet representation allows to describe the production

and decay structure with a minimum number of free parameters. Hence, the singlet representation was chosen as the most convenient and cleanest starting point to study the sensitivity of photon-induced singlet production processes in more isolation.

### 2.1 Signal Process and Final State

In the process under consideration, signal generation is addressed via a photon-induced mechanism based on the interaction between equivalent photons emitted from the muon beam and light up-type quarks in the parton content of the proton. At this point, it is well established that photon-induced processes serve as a powerful tool for new physics searches thanks to clean initial states and suppressed QCD backgrounds at high-energy colliders [51, 52]. Under the Equivalent Photon Approximation (EPA), the basic production sub-processes are realised as  $\gamma q(u, c) \rightarrow W^+ B$ . Accordingly, representative Feynman diagrams for these subprocesses are displayed in Fig. 1.

In addition, the full process description of the signal at the muonproton collision is

$$\mu p \rightarrow \mu \gamma p \rightarrow \mu W B X \rightarrow \mu W(Zb) X \rightarrow \mu \ell^+ \ell^- bjj X \quad (4)$$

The decay of the vector-like  $B$  quark generated in the above decay chain is analysed only as  $B \rightarrow Zb$  channel has been considered. Here, the leptonic decay channel ( $Z \rightarrow \ell^+ \ell^-$ ) of the generated  $Z$  boson is considered. Furthermore, the hadronic decay of the  $W$  boson accompanying the  $B$  quark is chosen as ( $W \rightarrow jj$ ) and thus the topology is ultimately obtained as  $\mu^+ \ell^+ \ell^+ \ell^- bjj$ . This final state offers low SM background and high invariant mass resolution thanks to leptonic  $Z$  decay, while hadronic  $W$  decay allows a complete reconstruction of the event topology. Taken together with the relatively clean environment provided by photon-induced production, this process offers a potentially highly selective and experimentally explorable environment for the search potential for vector-like  $B$  quarks.

### 2.2 Event Generation and Simulation Details

The production cross sections of the signal and SM background processes were calculated using the software package `MadGraph5_aMC@NLO`, which performs event generation at the parton level [53]. In the calculations, the vector-like  $B$  quark interactions are included in the

simulations through the appropriate UFO model defined in the framework of the simplified model [38, 50, 54–56]. Furthermore, after the event generation, the decays of the vector-like  $B$  quark are performed using the package **MadSpin** in such a way that spin correlations are preserved [57]. Thus, it is aimed to preserve the physical accuracy of the lepton and jet angular distributions, especially those arising from heavy resonance decays.

Kinematic cuts, invariant mass reconstructions and cut-flow analyses for the event selections have been performed using the **MadAnalysis 5** program framework [58]. These analyses allow us to evaluate a consistent and systematic comparison of signal and SM background processes.

In the calculations, the set **NNPDF3.1 NNLO** (LHAPDF ID: 303600) was used as parton distribution function (PDF) for the proton [59]. Also, the equivalent photon flux emitted from the muon beam was modelled using the Improved Weizsäcker–Williams (IWW) approximation [60]. This approach is widely used for the calculation of photon-induced processes at high-energy lepton-hadron colliders, and its reliability under modern collider conditions has been reported in detail in the literature [61].

In this context, the muon-induced photon distribution function is defined as follows,

$$f_{\gamma/\mu}(x) = \frac{\alpha}{2\pi} \left[ \frac{1 + (1-x)^2}{x} \ln\left(\frac{Q_{\max}^2}{Q_{\min}^2}\right) - 2(1-x) \right] \quad (5)$$

Accordingly, the total cross section of the photon-induced single  $B$  production in muon-proton collisions is calculated by the following equation, where the muon remains the spectator and the hadronic residues are represented by  $X$ .

$$\sigma(\mu p \rightarrow \mu WBX) = \sum_{q=u,c} \int dx_\gamma \int dx_q f_{\gamma/\mu}(x_\gamma) f_{q/p}(x_q, \mu_F) \hat{\sigma}(\gamma q \rightarrow WB) \quad (6)$$

Moreover, in our calculations, the production and decay processes are considered under the Narrow Width Approximation (NWA). In this approach, the production and decay of the heavy resonance in the calculation are factorised and thus the total cross section can be written as the product of the production cross section and the relevant branching ratios in the process [62–64]. This approximation is expressed as below,

$$\begin{aligned} & \sigma(\mu p \rightarrow \mu \ell^+ \ell^- b jj X) \\ &= \sigma(\mu p \rightarrow \mu \gamma p \rightarrow \mu WB) \\ & \quad \times \text{BR}(B \rightarrow Zb) \times \text{BR}(Z \rightarrow \ell^+ \ell^-) \times \text{BR}(W \rightarrow jj) \end{aligned} \quad (7)$$

The NWA approach is widely used in phenomenological analyses of vector-like quarks and is adopted as a standard assumption in singlet and pair production studies [1, 25, 27]. Since the condition  $\Gamma_B/M_B < 3\%$  is satisfied for the vector-like  $B$  quark in all parameter spaces analysed in our study, similar to the above literature, NWA can be considered to be safe and valid in the context of this study.

In this context, the signal cross section of the photon-induced single production of the vector-like  $B$  quark was calculated as a function of the mass  $M_B$  for different values of the coupling parameter  $g^*$ , and the results are presented in Fig. 2. As it can be seen from the figure, the production cross section decreases monotonically as  $M_B$  increases. On the other hand, it is observed that larger values of  $g^*$  significantly increase the production probabilities in the scanned mass range.

### 2.3 Standard Model Backgrounds and Event Selection

In order to ensure experimental distinguishability of the signal process, the kinematic and topological characteristics of the signal generation were first determined. Subsequently, Standard Model processes that can mimic the same final state as the signal process are also identified as background. Accordingly, a suitable event selection strategy was finally devised to effectively suppress these SM background contributions.

Here, three SM background processes are considered, which are occurred through the same photon-induced generation mechanism as the signal and make the dominant contribution to the cross section. In this context, for the final state  $\mu^+ \ell^+ \ell^- b jj$  under investigation, the dominant SM background processes are given by the following processes.

$$\gamma p \rightarrow WZj, \quad \gamma p \rightarrow WZb, \quad \gamma p \rightarrow ZZj \quad (8)$$

Accordingly, the distributions of some basic kinematic variables are presented in Fig. 3. As it is seen in Fig. 3(a) and Fig. 3(b), leptons and  $b$ -jets produced by the decay of the heavy  $B$  resonance are concentrated at higher transverse momentum ( $p_T$ ) values compared to background processes. In other words, signal events produce more energetic final-state particles. In contrast, the low- $p_T$  region is largely dominated by the  $WZj$

and  $ZZZj$  background processes. This kinematic separation suggests that the lower threshold  $p_T > 30$  GeV is an appropriate initial criterion for the selection of the basic object. This threshold effectively suppresses low-energy background contributions while it preserves a large fraction of the signal events.

On the other hand, Fig. 3(c) shows that for the angular separation variable  $\Delta R(b, \ell)$ , the signal events exhibit a significant concentration in the range  $3 \lesssim \Delta R(b, \ell) \lesssim 4$ . In contrast, the background processes, inhere, show a much wider angular distribution. In a brief, this behavior clearly demonstrates that the variable  $\Delta R(b, \ell)$  is a parameter that creates a significant difference between the signal and background processes. When the  $M_{b\ell\ell}$  invariant mass distributions presented in Fig. 3(d) are analysed, it is seen that a sharp resonance peak occurs for the signal. On the other hand, the background processes exhibit a monotonically decreasing and continuous distribution. These properties allow a direct reconstruction of the heavy  $B$  resonance.

Considering these kinematic features, selection cuts were sequentially applied to strengthen the signal-background separation as follows.

**Cut-1:** For detector acceptance and basic object selection,

- $p_T^\ell > 30$  GeV,  $|\eta^\ell| < 2.5$ ,
- $p_T^j > 30$  GeV,  $|\eta^j| < 2.5$ .

**Cut-2 (Angular Separation):**

$$3.2 < \Delta R(b, \ell) < 3.8$$

**Cut-3 (Boson Reconstruction):**

$$75 \text{ GeV} < M_{jj} < 85 \text{ GeV}, \quad 85 \text{ GeV} < M_{\ell\ell} < 95 \text{ GeV}$$

**Cut-4 (Heavy  $B$  Reconstruction):**

$$M_{\ell\ell b} > 1500 \text{ GeV}$$

At this point, the quantitative effects of the applied selection cuts on the signal and background processes are presented in Table 1. As it can be seen from the table, at the initial stage the background processes have cross sections several orders of magnitude higher than the signal. On the other hand, after the application of angular separation, boson reconstruction and high invariant mass cuts, the background contributions are strongly suppressed. However, the signal efficiency is preserved at about  $\sim 25\%$  for both mass values. These results clearly show that the chosen process and the applied cut strategy provide a highly selective and statistically robust analysis framework for the VLQ- $B$  discovery.

## 2.4 Statistical Analysis and Sensitivity

As it is well known, statistical significance calculations are required to quantitatively evaluate the effect of the distinction between the Signal and SM backgrounds on the discovery and exclusion potentials in terms of experimental sensitivity. Accordingly, for the significance of the discovery potential in our study, the expression based on the Asimov statistic given by Cowan et al. is adopted to quantify the discovery and exclusion sensitivities.

Here, the signal and background event numbers are defined sequentially as follows:

$$s = S = \sigma_S \times \mathcal{L} \times \prod_i \text{BR}_i \times \varepsilon_b \quad (9)$$

$$b = B = \sigma_B \times \mathcal{L} \times \prod_i \text{BR}_i \times \varepsilon_b \quad (10)$$

Here  $\sigma_S$  and  $\sigma_B$  correspond to the cross sections after the applied cuts for the signal and the total background, respectively. Furthermore,  $\mathcal{L}$  represents the integrated luminosity,  $\text{BR}_i$  the branching ratios of the corresponding decay channels, and  $\varepsilon_b$  the  $b$ -tagging efficiency. Since the discrimination of  $b$ -jets plays a critical role in the statistical analyses, the  $b$ -tagging efficiency for the signal and associated background processes is taken as  $\varepsilon_b = 0.85$ . This value is in agreement with the performances reported in LHC experiments in the high  $p_T$  regime and represents a realistic assumption considering the improved tracking and peak resolution expected in the next generation FCC-based colliders [65–67]. Furthermore, the high choice of  $\varepsilon_b$  ensures the protection of the vast majority of signal events, particularly due to the  $B \rightarrow Zb$  decay, while it also effectively suppresses background processes such as  $WZj$  and  $ZZj$  that contribute via spurious  $b$ -jet generation. When the background systematic uncertainty is denoted by  $\delta$ , the discovery significance is defined by the following equation [68]:

$$Z_{\text{disc}} = \left\{ 2 \left[ (s + b) \ln \left( \frac{(s + b)(1 + \delta^2 b)}{b + \delta^2 b(s + b)} \right) - \frac{1}{\delta^2} \ln \left( 1 + \frac{\delta^2 s}{1 + \delta^2 b} \right) \right] \right\}^{1/2} \quad (11)$$

This equation reduces to the following expression in the limit of  $\delta \rightarrow 0$ .

$$Z_{\text{excl}} = \left\{ 2 \left[ s - b \ln \left( \frac{b+s+x}{2b} \right) \right] - \frac{2}{\delta^2} \ln \left( \frac{b-s+x}{2b} \right) - (b+s-x) \left( 1 + \frac{1}{\delta^2 b} \right) \right\}^{1/2} \quad (12)$$

Where  $x$  parameter is defined as  $x = \sqrt{(s+b)^2 - \frac{4\delta^2 s b^2}{1+\delta^2 b}}$ . Also, in the limit  $\delta \rightarrow 0$ , the exclusion significance takes the following form.

$$Z_{\text{excl}} = \sqrt{2 \left[ s - b \ln \left( 1 + \frac{s}{b} \right) \right]} \quad (13)$$

In the current study, the significance threshold for signal discovery is  $Z_{\text{disc}} \geq 5$  (equivalent to  $5\sigma$ ). Additionally, the exclusion significance were defined based on the  $Z_{\text{excl}} \geq 1.65$  condition (approximately 95% confidence level) corresponding to a one-sided Gaussian distribution. Using these thresholds, the statistical significance values in the  $g^* M_B$  parameter space was calculated separately for the  $\delta = 0$  and  $\delta = 0.10$  cases, representing the systematic uncertainty in the number of background events. The obtained results are presented comparatively in Figs. 4 and 5. In Fig. 4, the expected discovery reach of  $5\sigma$  in the  $g^* st - M_B$  plane for  $\varepsilon_b = 0.85$  is shown under two different systematic uncertainty assumptions and integrated luminosity values of  $\mathcal{L} = 400$  and  $1000 \text{ fb}^{-1}$ . As it can be seen from the figure, as  $M_B$  increases, the minimum  $g^*$  required for exploration increases approximately linearly. Moreover, it is observed that increasing the integrated luminosity from  $400$  to  $1000 \text{ fb}^{-1}$  significantly improves the discovery reach. In this context, the results obtained at different mass values for  $5\sigma$  discovery reach are analysed in detail. For an integrated luminosity of  $\mathcal{L} = 1000 \text{ fb}^{-1}$ , the minimum coupling required for a  $5\sigma$  discovery is found to be  $g^* \simeq 0.223$  at  $M_B = 2000 \text{ GeV}$ , increasing to  $g^* \simeq 0.296$  at  $M_B = 3000 \text{ GeV}$ . For the lower integrated luminosity scenario of  $\mathcal{L} = 400 \text{ fb}^{-1}$ , the corresponding discovery limits weaken to  $g^* \simeq 0.298$  and  $g^* \simeq 0.396$ , respectively. These results clearly show that increasing the integrated luminosity significantly enhances the discovery potential, especially in high-mass regions. Furthermore, a similar behaviour tendency to Fig. 4 is observed in Fig. 5, which shows the exclusion limits at 95% C.L. in the same parameter space. In other words, it is also clearly seen that the smaller  $g^*$  coupling values with higher values of integrated luminosity can be excluded. In this graph, it can be seen that for  $\mathcal{L} = 1000 \text{ fb}^{-1}$ , the exclusion limits of the coupling constant values at mass values  $M_B = 2000 \text{ GeV}$

and  $M_B = 3000 \text{ GeV}$  are also reduced to  $g^* \simeq 0.125$  and  $g^* \simeq 0.167$ , respectively. At the same mass values for the lower integrated luminosity  $\mathcal{L} = 400 \text{ fb}^{-1}$ , the exclusion limits increase slightly, reaching  $g^* \simeq 0.167$  and  $g^* \simeq 0.223$ , respectively. In other words, these exclusion limits weaken. This comparison for the two luminosity values indicates that the increase in integrated luminosity directly and significantly improves the exclusion power. In both figures, it can be said that the difference between the  $\delta = 0$  and  $\delta = 10\%$  scenarios is quite small. This is mainly due to the fact that the background contributions are suppressed by several orders of magnitude after the applied kinematic cuts and thus, the statistical significance is largely determined by the number of signal events. This situation indicates that statistical uncertainties dominate the analysis, while the effect of systematic uncertainty is secondary. Hence, in all the remaining sensitivity analyses of the study, the case  $\delta = 0$  is adopted to simplify the statistical interpretation. Furthermore, we analysed the luminosity dependence of the branching ratio and the obtained results were presented in Fig. 6. Here, the minimum values of  $\text{BR}(B \rightarrow Zb)$  required for  $5\sigma$  discovery reach and 95% C.L. exclusion limits are presented in the range of  $\mathcal{L} = 400\text{--}1000 \text{ fb}^{-1}$ . Moreover,  $M_B = 2000 \text{ GeV}$  and  $g^* = 0.2$  were chosen in the calculations. Accordingly, when the figure is examined, it is observed that the  $\text{BR}(B \rightarrow Zb)$  values decrease as the integrated luminosity increases. Also,  $\text{BR}(B \rightarrow Zb)$  values for  $5\sigma$  discovery reach at  $\mathcal{L} = 400 \text{ fb}^{-1}$  are about 0.55, while the values at  $\mathcal{L} = 1000 \text{ fb}^{-1}$  decrease to 0.35. Similarly,  $\text{BR}(B \rightarrow Zb)$  values for the exclusion limit at the 95% confidence level decrease from about 0.25 to 0.11. These findings indicate that increasing integrated luminosity at the FCC- $\mu\mu$  collider significantly improves the accessibility of scenarios with smaller  $\text{BR}(B \rightarrow Zb)$  values. After examining the dependence of the branching ratio on the integrated luminosity, the sensitivity of  $\text{BR}(B \rightarrow Zb)$  to the VLQ- $B$  mass was also investigated. The corresponding  $5\sigma$  discovery reach and 95% C.L. exclusion limits as a function of  $M_B$  are presented in Fig. 7. Examining the figure, it is observed that as the  $M_B$  values increase, the  $\text{BR}(B \rightarrow Zb)$  values required for both discovery and exclusion increase monotonically. This behavioral trend can be attributed to the quick decrease in the production cross-section of VLQ- $B$  in the heavy mass regime. Furthermore, it is observed that the  $\text{BR}(B \rightarrow Zb)$  values required for discovery are above the exclusion limits for all mass values considered in the calculations. For example,  $\text{BR}(B \rightarrow Zb)$  values for the exclusion limit at 95% C.L. at  $M_B \simeq 1800 \text{ GeV}$ , are approximately 0.20, while the values for the  $5\sigma$  discovery reach are 0.30. Similarly,  $\text{BR}(B \rightarrow Zb)$  values

required at  $M_B \simeq 3000$  GeV reach approximately 0.45 and 0.60 for the exclusion limit and discovery reach states, respectively. These results indicate that in the heavy-mass regime the discovery reach requires higher  $\text{BR}(B \rightarrow Zb)$  values than the exclusion limit and that is, is experimentally more difficult to observe. When the sensitivity analysis findings obtained are compared with existing studies in the literature, it can be concluded that the  $\sqrt{s} = 24.5$  TeV photon-induced single production scenario considered in this study provides a significant advantage for massive VLQ- $B$  discovery studies. For example, in direct discovery searches conducted with LHC Run-2 data by ATLAS and CMS collaborations, exclusion limits at 95% C.L. via the pair production channel were reported as  $M_B \simeq 1.2\text{--}1.6$  TeV. On the other hand, in single production analyses, the sensitivity analyses were found to be strongly dependent on the coupling parameter and also the exclusion limits at 95% C.L. were obtained in the  $M_B \lesssim 1.0\text{--}1.4$  TeV region. In summary, it can be said that the LHC environment rapidly makes single VLQ- $B$  production in the  $M_B > 2$  TeV regime inaccessible. On the other hand, in the context of Lepton-hadron colliders, sensitivity analyses on LHeC and FCC-eh for  $B \rightarrow Zb$  decay have reported exclusion potentials in the range  $M_B \sim 1.4\text{--}2.2$  TeV. Accordingly, due to their limited center-of-mass energies, the production cross sections in LHeC and FCC-eh can be expected to decrease rapidly for heavier masses. Similarly, single VLQ- $B$  production in the 3 TeV CLIC scenario offers discovery access around  $M_B \sim 2$  TeV, however it is reported that the discovery potential for  $M_B \gtrsim 2.7$  TeV significantly weakened due to the electroweak-scale production mechanism of VLQ- $B$ . Comparing the results of the above literature with the results of the present work, it is predicted that the FCC- $\mu p$  photon-induced single production mechanism considered in this work can maintain its efficiency even in the heavy-mass regime due to the advantage of high center-of-mass energy and can be accessible even at small coupling constant values used in the  $M_B = 2\text{--}3$  TeV region. For example, for  $\mathcal{L} = 1000 \text{ fb}^{-1}$ , the obtained exclusion limits at the 95% C.L. drop to the value range of  $g^* \simeq 0.12\text{--}0.17$ . Even the  $5\sigma$  discovery reach remain at the  $g^* \simeq 0.22\text{--}0.30$  value level. These obtained sensitivity values go several TeV beyond the current experimental reach of the LHC. Moreover, they provide complementary predictions to the phenomenological sensitivity of the ep and  $e^+e^-$  colliders, which rapidly weakens at high masses. To summarise, this study provides a significant sensitivity analysis for the heavy VLQ- $B$  discovery of the FCC- $\mu p$  environment that both goes beyond the LHC limits and complements the high-mass reach of future ep and lepton colliders.

### 3 Conclusion

In this work, the photon-induced single production of the vector-like singlet type  $B$  quark in a FCC- $\mu p$ -based muon-proton collider at a centre-mass energy of  $\sqrt{s} = 24.5$  TeV is investigated in detail. To this end, the presented analyses, herein, consider the  $B \rightarrow Zb$  decay. The final state  $\mu^+\ell^+\ell^+\ell^-bjj$  is analysed by choosing the leptonic channel of the  $Z$  boson and the hadronic channel of the  $W$  boson that accompanies this decay. The attraction of this process of interest is that it offers a selective final state with high discrimination between the signal and background processes thanks to its low QCD background, narrow resonance structures, and efficient  $b$ -labeling. In this context, the analyses revealed that the applied kinematic cuts suppressed the SM backgrounds by several orders of magnitude and signal efficiency was also preserved at the  $\sim 25\%$  level. In a brief, it can be said according to these findings that our analysis strategy indicates an effective and balanced selection for the heavy mass regime. In the study, statistical analyses were performed under the Asimov approach and it was concluded that the background systematic uncertainty has a negligible effect on the discovery and exclusion sensitivities between the  $\delta = 0$  and  $\delta = 10\%$  scenarios. This observation suggests that the statistical significance is largely governed by the number of signalling events. Furthermore, the obtained results indicate a tighten sensitivity in the parameter space  $g^* \text{-} M_B$ . For  $\mathcal{L} = 1000 \text{ fb}^{-1}$  and in the range of  $M_B = 2\text{--}3$  TeV, the  $5\sigma$  discovery reach values are  $g^* \simeq 0.22\text{--}0.30$  and the exclusion limits at 95% confidence level go down to  $g^* \simeq 0.12\text{--}0.17$ . These results demonstrate that these obtained values offer a complementary reach extending several TeV beyond the current LHC Run-2 experimental limits.

Furthermore, sensitivities in terms of  $\text{BR}(B \rightarrow Zb)$  were also examined to provide a perspective independent of coupling parameters. At this point, it was observed that with increasing integrated luminosity, the minimum  $\text{BR}(B \rightarrow Zb)$  required for discovery and exclusion decreased significantly. In particular, for  $\mathcal{L} = 1000 \text{ fb}^{-1}$ , at  $M_B \simeq 2$  TeV, VLQ- $B$  is discovery level with  $\text{BR}(B \rightarrow Zb) \sim 0.3$  while it is seen at heavier masses that the required minumun  $\text{BR}(B \rightarrow Zb)$  values rapidly increases. This situation can be attributed to the decrease in the production cross-section in the heavy mass regime. In conclusion, the findings of this study clearly demonstrate that the photon-induced single production mechanism in the FCC- $\mu p$  environment offers a unique and complementary exploration framework for heavy VLQ- $B$  discovery. Furthermore, the obtained sensitivities effectively complement the dimin-

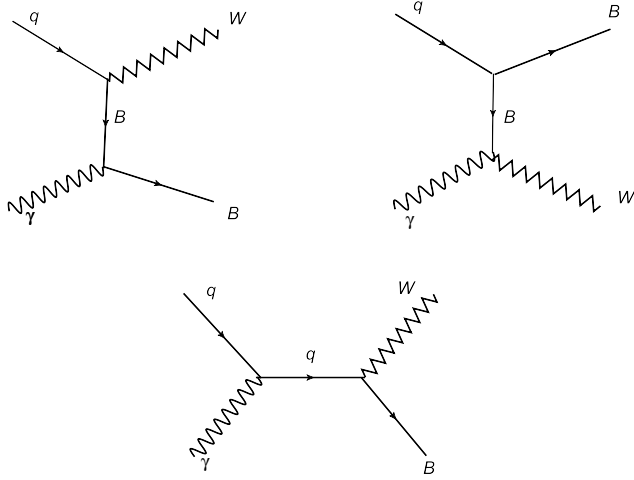


**Fig. 1** Tree-level Feynman diagrams for the photon-induced subprocesses  $\gamma q (q = u, c) \rightarrow W^+ B$ .

ishing reach of the LHC, ep, and  $e^+e^-$  colliders in the high-mass regime, and thus indicate that  $\mu p$  machines can play not only a complementary but also a decisive role in the search for new physics. In this context, it is predicted that  $\mu p$  colliders will stand out as a strategic component in the future accelerator program for the search for new heavy particles and will be a powerful experimental tool for the exploration of physics beyond the SM.

### Acknowledgements

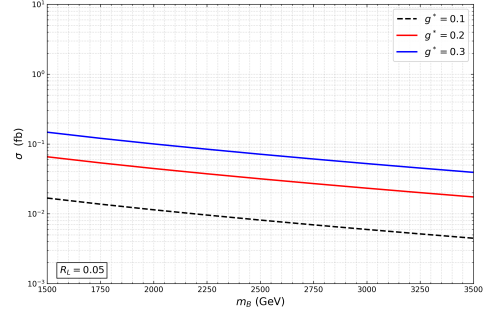
This work was supported by the Scientific Research Projects Coordination Unit of Zonguldak Bülent Ecevit University under Project No. 2025-22794455-04.

### Data Availability Statement

This study is based on Monte Carlo simulations performed using the MADGRAPH framework. No experimental data were generated or analyzed in this study.

### Code Availability Statement

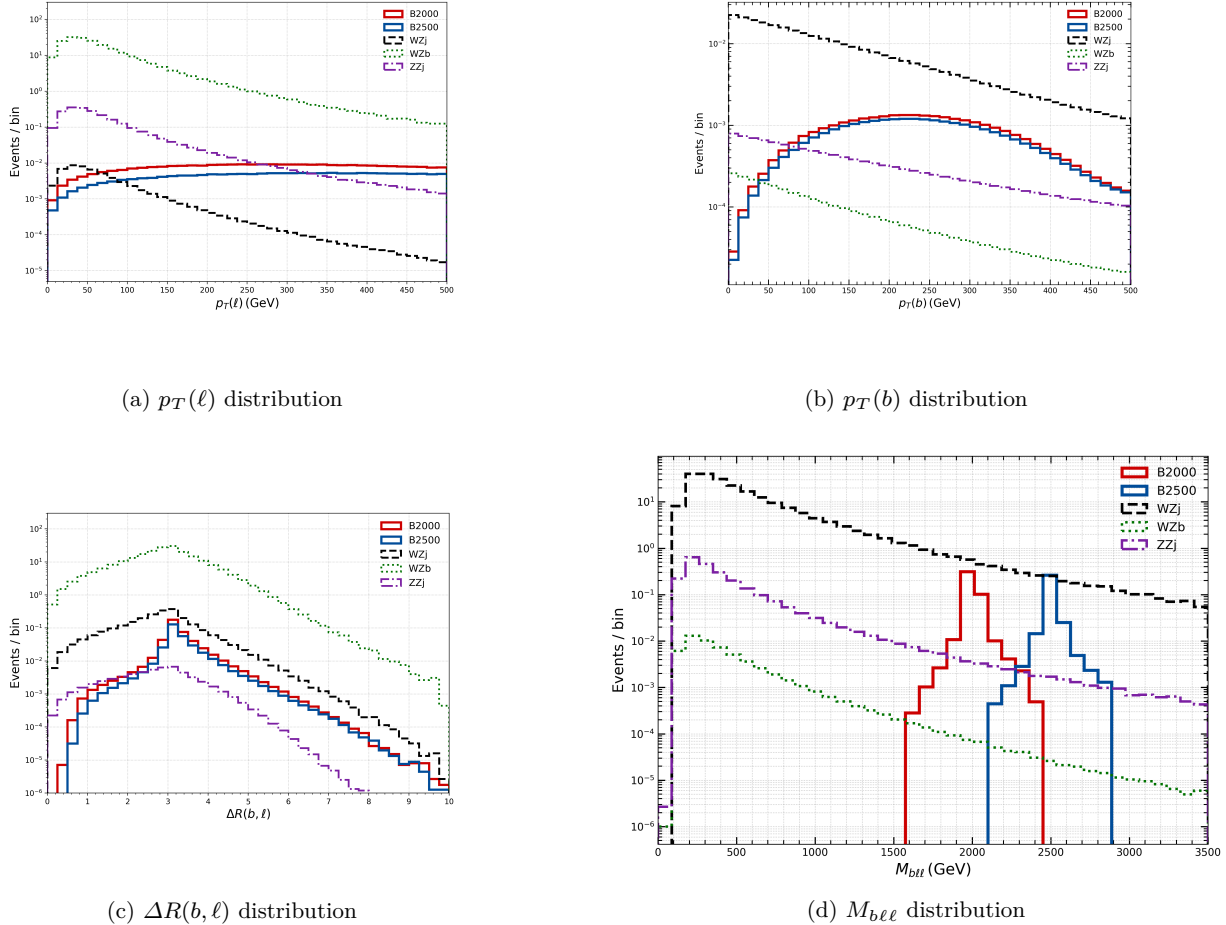
No new code was developed in this study. All simulations were performed using the publicly available MADGRAPH framework.



**Fig. 2** Production cross section of the photon-induced main process as a function of the vector-like  $B$  quark mass for different values of the coupling parameter  $g^*$ .

**Table 1** Cut-flow table for the signal and background processes at an integrated luminosity of  $\mathcal{L} = 1000 \text{ fb}^{-1}$ .

Cuts	Signal ( $M_B = 2000$ )	Signal ( $M_B = 2500$ )	$WZj$	$WZb$	$ZZj$
Basic Cut	$4.45 \times 10^{-5}$	$3.17 \times 10^{-5}$	$2.20 \times 10^{-2}$	$5.65 \times 10^{-6}$	$2.39 \times 10^{-4}$
Cut 1	$1.48 \times 10^{-5}$	$1.10 \times 10^{-5}$	$4.20 \times 10^{-3}$	$9.23 \times 10^{-7}$	$3.98 \times 10^{-5}$
Cut 2	$1.12 \times 10^{-5}$	$8.30 \times 10^{-6}$	$1.27 \times 10^{-4}$	$7.03 \times 10^{-7}$	$6.45 \times 10^{-7}$
Cut 3	$1.12 \times 10^{-5}$	$8.30 \times 10^{-6}$	$4.28 \times 10^{-6}$	$2.46 \times 10^{-8}$	$9.59 \times 10^{-9}$
Efficiency (%)	25.2	26.1	$1.95 \times 10^{-2}$	$4.35 \times 10^{-1}$	$4.01 \times 10^{-3}$

**Fig. 3** Distributions of the main kinematic variables used in the analysis for the signal and background processes.

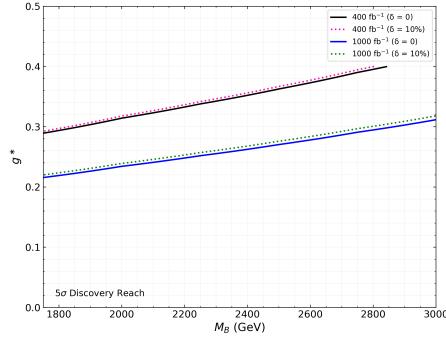


**Fig. 4** Expected  $5\sigma$  discovery reach in the  $g^*$ – $M_B$  plane for integrated luminosities of  $\mathcal{L} = 400$  and  $1000 \text{ fb}^{-1}$ , considering the cases of  $\delta = 0$  and  $\delta = 10\%$ .

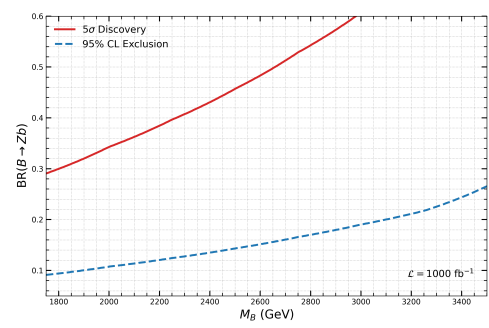


**Fig. 7** Branching ratio  $\text{BR}(B \rightarrow Zb)$  as a function of the vector-like  $B$  quark mass for  $g^* = 0.2$  at an integrated luminosity of  $\mathcal{L} = 1000 \text{ fb}^{-1}$ .

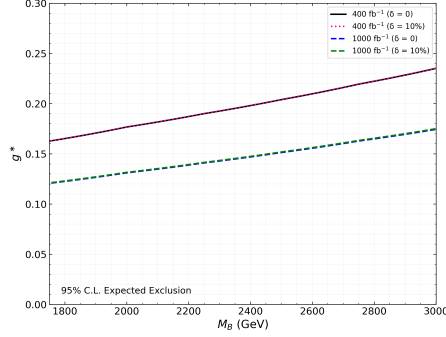


**Fig. 5** Expected 95% confidence level exclusion contours in the  $g^*$ – $M_B$  plane for integrated luminosities of  $\mathcal{L} = 400$  and  $1000 \text{ fb}^{-1}$  considering the cases of  $\delta = 0$  and  $\delta = 10\%$ .

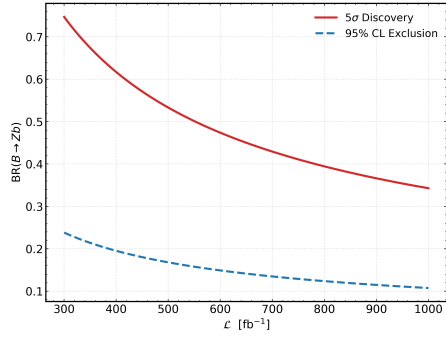


**Fig. 6** Required  $\text{BR}(B \rightarrow Zb)$  as a function of the integrated luminosity for the  $5\sigma$  discovery reach and the 95% confidence level exclusion limit at  $M_B = 2000 \text{ GeV}$  and  $g^* = 0.2$ .

## References

- J. A. Aguilar-Saavedra. Identifying top partners at the LHC. *JHEP*, 2009(11):030, 2009.
- G. Cacciapaglia, A. Deandrea, and L. Panizzi. Vector-like quarks: models and phenomenology. *JHEP*, 2012(03):070, 2012.
- G. Cacciapaglia, A. Deandrea, D. Harada, and Y. Okada. Bounds and decays of new heavy vector-like top partners. *JHEP*, 2010(11):159, 2010.
- Anupama Atre, Georges Azuelos, Marcela Carena, Tao Han, Erkcan Ozcan, Jose Santiago, and Gokhan Unel. Model-independent searches for new quarks at the lhc. *JHEP*, 2011(08):080, 2011.
- Mikael Chala, Ramona Gröber, and Michael Spannowsky. Searches for vector-like quarks at future colliders and implications for composite higgs models with dark matter. *JHEP*, 2018(03):040, 2018.
- B.-F. Yang, B.-F. Hou, H.-Y. Zhang, and N. Liu. Single production of vector-like top partner decaying to  $wb$  in the leptonic channel at  $ep$  colliders in the littlest higgs model with  $t$ -parity. *Phys. Rev. D*, 99:095002, 2019.
- A. Angelescu, A. Djouadi, and G. Moreau. Vector-like top/bottom quark partners and higgs physics at the lhc. *Eur. Phys. J. C*, 76:99, 2016.
- Ning Liu, Lei Wu, Bingfang Yang, and Mengchao Zhang. Single production of the t-even top partner in the littlest higgs model with t-parity. *Phys. Lett. B*, 753:664–669, 2016.
- Chuan-Hung Chen and Takaaki Nomura. Single production of  $x_{\pm 5/3}$  and  $y_{\mp 4/3}$  vectorlike quarks at the lhc. *Phys. Rev. D*, 94:035001, 2016.
- Alexandra Carvalho, Stefano Moretti, Dermot O'Brien, Luca Panizzi, and Hugo Prager. Single production of vector-like quarks with large width at the large hadron collider. *Phys. Rev. D*, 98:015029, 2018.
- A. Banerjee, V. Ellajosyula, and L. Panizzi. Heavy vector-like quarks decaying to exotic scalars: a case study with triplets. *JHEP*, 2024(01):187, 2024.
- J. Bardhan, T. Mandal, S. C. Mitra, and C. Neeraj. Machine learning enhanced search for vectorlike single  $b$  quark decaying to a single scalar or pseudoscalar. *Phys. Rev. D*, 107:115001, 2023.
- D. Barducci and L. Panizzi. Vector-like quarks coupling discrimination at the lhc and future hadron colliders. *JHEP*, 2017(12):057, 2017.
- A. C. Canbay and O. Cakir. Investigating the single production of vectorlike quarks decaying into a top quark and  $w$  boson through hadronic channels at the HLLHC. *Phys. Rev. D*, 108:095006, 2023.
- A. Banerjee, E. Bergeas Kuutmann, V. Ellajosyula, R. Enberg, G. Ferretti, and L. Panizzi. Vector-like quarks: status and new directions at the lhc. *SciPost Phys. Core*, 7:079, 2024.
- Y.-B. Liu, B. Hu, and C.-Z. Li. Single production of vector-like quarks with charge  $5/3$  at the 14 tev lhc. *Nucl. Phys. B*, 1007:116667, 2024.
- Y.-J. Zhang, Y.-P. Liu, Y.-T. Zhu, Y.-P. Bi, and T.-G. Liu. Searching for the vector-like  $x$ -quark at the future electron-proton colliders. *Eur. Phys. J. C*, 84:13475, 2024.
- B.-F. Yang, M. Wang, H. Bi, and L. Shang. Single production of vectorlike  $t$  quark decaying into  $wb$  at the lhc and the future  $pp$  colliders. *Phys. Rev. D*, 103:036006, 2021.
- V. Cetinkaya, A. Ozansoy, V. Ari, O. M. Ozismek, and O. Cakir. Single production of vector-like  $y$  quarks at the HL-LHC. *Nucl. Phys. B*, 973:115580, 2021.
- H. Zhou and N. Liu. Probing a new decay mode of a vectorlike top partner mediated by a heavy majorana neutrino via gluon fusion. *Phys. Rev. D*, 101:112028, 2020.
- Y.-B. Liu. Search for single production of the heavy vector-like  $t$  quark with  $t \rightarrow th$  and  $t \rightarrow \gamma t$  at the high-luminosity LHC. *Phys. Rev. D*, 95:035013, 2017.
- G.-S. Lv, X.-M. Cui, and Y.-Q. Li. Pair production of vector-like top partner at future muon colliders. *Nucl. Phys. B*, 985:116016, 2022.
- X. Qin, L.-F. Du, and J.-F. Shen. Single production of vector-like  $t$  quark decaying into  $wb$  at the clic. *Nucl. Phys. B*, 979:115784, 2022.
- J.-Z. Han, Y.-B. Liu, and S. Moretti. Searching for single production of vector-like quarks decaying into  $wb$  at a future muon-proton collider. *arXiv e-prints*, 2025.
- X. Gong, C.-X. Yue, and Y.-C. Guo. Search for vector-like bottom quark via  $zb$  production at the lhc. *Phys. Lett. B*, 793:175–180, 2019.
- B. Yang, Z. Li, X. Jia, S. Moretti, and L. Shang. Search for single vector-like  $b$  quark production in hadronic final states at the LHC. *Eur. Phys. J. C*, 84:1124, 2024.
- J.-Z. Han, Y.-B. Liu, L. Xing, and S.-Y. Xu. Search for single production of vectorlike  $b$ -quarks at the lhc. *Chin. Phys. C*, 46:103103, 2022.
- J.-Z. Han, J. Yang, S.-Y. Xu, and H.-K. Wang. Search for single production of vector-like  $b$  quark via  $bz$  channel at the HL-LHC. *Nucl. Phys. B*, 975:115672, 2022.
- A. De Simone, O. Matsedonskyi, R. Rattazzi, and A. Wulzer. A first top partner hunters guide. *JHEP*, 2013(04):004, 2013.
- Q.-G. Zeng, Y.-S. Pan, and J. Zhang. Search for the signal of vector-like bottom quark at the LHeC in the final state with three  $b$  jets. *Nucl. Phys. B*, 995:116347, 2023.
- X. Gong, C.-X. Yue, H.-M. Yu, and D. Li. Single production of vector-like bottom quark at the LHeC. *Eur. Phys. J. C*, 80:780, 2020.
- L. Shang, C. Chen, S. Wang, and B. Yang. Single production of vector-like  $b$  quark decaying into  $bz$  at future  $ep$  colliders. *Nucl. Phys. B*, 984:115977, 2022.
- J.-Z. Han, J. Yang, S. Xu, and H.-K. Wang. Single production of vectorlike  $b$  quarks at the CLIC. *Phys. Rev. D*, 105:015005, 2022.
- J.-Z. Han, Y.-B. Liu, and S.-Y. Xu. Pair production of the singlet vectorlike  $b$  quark at the clic. *Eur. Phys. J. C*, 84:61, 2024.
- S. Yang, Y.-H. Wang, P.-B. Zhao, and J.-L. Ma. Searching for heavy vector-like  $b$  quark via pair production in fully hadronic channels at CLIC. *arXiv e-prints*, 2025.
- H.-J. He, Y.-P. Kuang, and X.-Y. Li. On the precise formulation of the equivalence theorem. *Phys. Rev. Lett.*, 69:2619–2622, 1992.
- H.-J. He, Y.-P. Kuang, and X.-Y. Li. Further investigation on the precise formulation of the equivalence theorem. *Phys. Rev. D*, 49:4842–4872, 1994.
- M. Buchkremer, G. Cacciapaglia, A. Deandrea, and L. Panizzi. Model-independent framework for searches of top partners. *Nucl. Phys. B*, 876:376–417, 2013.
- J. A. Aguilar-Saavedra, R. Benbrik, S. Heinemeyer, and M. Perez-Victoria. A handbook of vector-like quarks: mixing and single production. *Phys. Rev. D*, 88:094010, 2013.
- ATLAS Collaboration. Search for single production of a vector-like  $b$  quark and decay via  $b \rightarrow bh(b\bar{b})$  in  $pp$  collisions at  $\sqrt{s} = 13$  tev. *JHEP*, 11:168, 2023.
- ATLAS Collaboration. Search for pair-produced vectorlike quarks coupling to light quarks in the lepton plus jets final state using 13 tev  $pp$  collisions with the atlas detector. *Phys. Rev. D*, 110:052009, 2024.

42. CMS Collaboration. Search for pair production of vector-like quarks in the fully hadronic final state. *Phys. Rev. D*, 100:072001, 2019.

43. CMS Collaboration. Search for pair production of vector-like quarks in leptonic final states in proton-proton collisions at  $\sqrt{s} = 13$  tev. *JHEP*, 07:020, 2023.

44. CMS Collaboration. Review of searches for vector-like quarks, vector-like leptons, and heavy neutral leptons in proton-proton collisions at  $\sqrt{s} = 13$  tev. *Phys. Rept.*, 1115:570–677, 2025.

45. K. Cheung et al. Physics potential of muon–proton colliders. *Phys. Rev. D*, 105:015007, 2022.

46. J. P. Delahaye et al. Muon colliders, 2019.

47. A. Abada et al. FCC physics opportunities: Future Circular Collider conceptual design report Volume 1. *Eur. Phys. J. C*, 79:474, 2019.

48. K. R. Long et al. Muon colliders to expand frontiers of particle physics. *Nature Phys.*, 17:289–292, 2021.

49. M. Benedikt, F. Zimmermann, et al. Future circular collider feasibility study report: Volume 2. *Eur. Phys. J. Special Topics*, 234:5713–6197, 2025.

50. J. A. Aguilar-Saavedra, J. De Blas, and M. Perez-Victoria. Effective field theory approach to vector-like quarks. *Phys. Rev. D*, 88:094010, 2013.

51. K. Piotrzkowski. Tagging two-photon production at the CERN LHC. *Phys. Rev. D*, 63:071502, 2001.

52. S. Fichet, G. von Gersdorff, B. Lenzi, C. Royon, and M. Saimpert. Light-by-light scattering with intact protons at the lhc: from standard model to new physics. *Phys. Rev. D*, 91:075006, 2015.

53. J. Alwall, R. Frederix, S. Frixione, V. Hirschi, F. Maltoni, O. Mattelaer, H.-S. Shao, T. Stelzer, P. Torrielli, and M. Zaro. The automated computation of tree-level and NLO cross sections and their matching to parton shower simulations. *JHEP*, 2014(07):079, 2014.

54. C. Degrande, C. Duhr, B. Fuks, D. Grellscheid, O. Mattelaer, and T. Reiter. UFO – the universal FeynRules output. *Comput. Phys. Commun.*, 183:1201–1214, 2012.

55. A. Alloul, N. D. Christensen, C. Degrande, C. Duhr, and B. Fuks. FeynRules 2.0 – a complete toolbox for tree-level phenomenology. *Comput. Phys. Commun.*, 185:2250–2300, 2014.

56. FeynRules VLQ Model Repository. Singlet  $b$  vector-like quark model. [https://feynrules.irmp.ucl.ac.be/wiki/VLQ\\_bsingletvl](https://feynrules.irmp.ucl.ac.be/wiki/VLQ_bsingletvl), 2014. Accessed 2 Feb 2024.

57. P. Artoisenet, R. Frederix, O. Mattelaer, and R. Rietkerk. Automatic spin-entangled decays of heavy resonances in monte carlo simulations. *JHEP*, 2013(03):015, 2013.

58. E. Conte, B. Fuks, and G. Serret. MadAnalysis 5, a user-friendly framework for collider phenomenology. *Comput. Phys. Commun.*, 184:222–256, 2013.

59. R. D. Ball et al. Parton distributions from high-precision collider data. *Eur. Phys. J. C*, 77:663, 2017.

60. V. M. Budnev, I. F. Ginzburg, G. V. Meledin, and V. G. Serbo. The two-photon particle production mechanism. physical problems. applications. equivalent photon approximation. *Phys. Rept.*, 15(4):181–282, 1975.

61. M. Klasen, B. A. Kniehl, and L. Mihaila. Photon-induced processes at high-energy colliders. *Phys. Rev. D*, 89:014012, 2014.

62. N. Kauer. Narrow-width approximation limitations. *Phys. Lett. B*, 649:413, 2007.

63. D. Berdine, N. Kauer, and D. Rainwater. Breakdown of the narrow width approximation for new physics. *Phys. Rev. Lett.*, 99:111601, 2007.

64. N. Kauer and G. Passarino. Inadequacy of the zero-width approximation for a light higgs boson signal. *JHEP*, 08:116, 2012.

65. ATLAS Collaboration. Performance of  $b$ -jet identification in the ATLAS experiment. *JINST*, 11:P04008, 2016.

66. CMS Collaboration. Identification of heavy-flavour jets with the CMS detector in pp collisions at 13 TeV. *JINST*, 13:P05011, 2018.

67. F. Bedeschi, L. Gouskos, and M. Selvaggi. Jet flavour tagging for future colliders with fast simulation. *Eur. Phys. J. C*, 82:646, 2022.

68. G. Cowan, K. Cranmer, E. Gross, and O. Vitells. Asymptotic formulae for likelihood-based tests of new physics. *Eur. Phys. J. C*, 71:1554, 2011.